Journal of Ovonic Research Vol. 20, No. 5, September - October 2024, p. 601 - 615

DFT study of elastic and thermodynamic properties of solar material Cu_2ZnSnS_4

S. H. Fan[a,*], H. J. Hou[a], H. L. Guo[b]
[a]*School of Materials Science and Engineering, Yancheng Institute of Technology, Yancheng, 224051, China*
[b]*College of Electronic and Information Engineering, Yangtze Normal University, Fuling, 408000, Chongqing, China*

In this study, the mechanical characteristics of Cu_2ZnSnS_4 are investigated under varying pressures. The correlations between pressure and elastic constants C_{ij}, bulk modulus B, shear modulus G, and Young's modulus E, are obtained. The thermal properties of Cu_2ZnSnS_4 were studied, including Debye temperature θ, heat capacity C_V and C_P, thermal expansion coefficient α, Grüneisen constant γ and entropy S at temperatures (0, 200, 400, 600, 800, 1000, 1200K) and pressures (0, 2, 4, 6, 8, 10 GPa), are also obtained and analyzed.

(Received June 18, 2024; Accepted September 11, 2024)

Keywords: Cu_2ZnSnS_4, Elastic properties, Thermal properties

1. Introduction

With the swift advancement of human society, economic and cultural integration, energy, environmental protection and other hidden problems also slowly surface, one of the most cannot be ignored is the problem of energy shortage, so developing new energy sources is the most urgent thing at present [1]. Solar energy is both inexhaustible and stable and clean, making it one of the most efficient and promising alternative energy sources [2]. Among them, Cu_2ZnSnS_4 as the material of the new solar thin film battery is the most outstanding [3]. Prior to the 1960s, the study of semiconductors was focused on monadic, binary, and ternary semiconductors because of technology and capability constraints, but after 1960, more and more researchers have noticed the Cu_2ZnSnS_4 type I_2-II-IV-VI_4 quaternary semiconductor, which has the advantages of non-toxic, large reserves, environmental protection, high theoretical efficiency and suitable band gap, it has great potential as a photocatalyst and solar cell [4, 5]. Therefore, in recent years, the Cu_2ZnSnS_4 has become a hot research topic in the new generation of Photovoltaic cells with thin films. Meanwhile, the band gap width of Cu_2ZnSnS_4 is about 1.5 eV, which is consistent with the optimal band gap of solar cell and has a competitive advantage over other list of semiconductor materials. Although there are relevant experimental and theoretical studies on Cu_2ZnSnS_4. As far as we know, the elastic properties of Cu_2ZnSnS_4 under pressure have not been systematically obtained [6]. Pressure has an important effect on the stress or strain characteristics of solids, so it is important to explore the elastic and thermal characteristics of Cu_2ZnSnS_4 to clarify the mechanical properties of materials under pressure.

* Corresponding author: dahaitg@163.com
https://doi.org/10.15251/JOR.2024.205.601

2. Calculation methods

The structural and elastic characteristics of Cu_2ZnSnS_4 are obtained using the CASTEP code, which employs plane wave pseudopotentials [7]. In our calculation, we employ the Perdew-Burke-Ernzerhof (PBE) generalized gradient approximation (GGA)[8] to determine the exchange correlation potential. Additionally, for the considered structure, we utilize Vanderbilt ultrasoft pseudopotential [9] with a cutoff energy of 600 eV. The Monkhorst-Pack scheme is utilized to generate the *k* point meshes of Cu_2ZnSnS_4, with a size of 5×5×5.

3. Results and discussion

3.1 Structural properties

Cu_2ZnSnS_4 belongs to the family of quaternary chalcogenide semiconductors with an I_2-II-IV-VI_4 crystal structure. The space group of Cu_2ZnSnS_4 is I-42m, the serial number is 121, the coordinates of Cu is (0, 0.5, 0.25), the coordinates of Zn is (0, 0, 0), and the coordinates of Sn is (0, 0, 0.5), the coordinates of S is (0.258, 0.258, 0.3714). Fig. 1. shows the structural model of Cu_2ZnSnS_4.

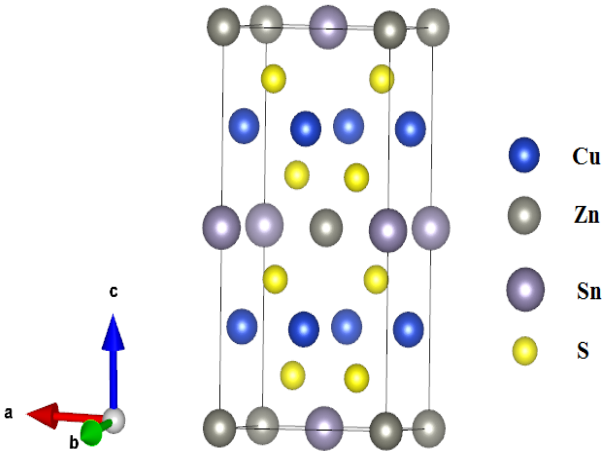

Fig. 1. Structural model of Cu_2ZnSnS_4.

Table 1. The current lattice constants of Cu_2ZnSnS_4, as determined through using different functionals.

	LDA	GGA-RPBE	GGA-PBE	GGA-PW91	GGA-PBESOL	Exp.[10]
$a = b$(Å)	5.3421	5.5718	5.4301	5.4391	5.3787	5.449
c (Å)	10.8718	11.3787	10.8965	11.6401	11.5169	10.757
a, b relative error	1.96%	2.25%	0.035%	0.18%	1.29%	0
c relative error	1.06%	5.77%	1.29%	8.21%	7.06%	0

Table 1 shows the results of the optimization of Cu_2ZnSnS_4 by different methods, the errors of *a* (*b*) and *c* of LDA, GGA-RPBE, GGA-PBE, GGA-PW91, GGA-PBESOL were 1.96% and 1.06%, 2.25% and 5.77%, 0.035% and 1.29%, 0.18% and 8.21%, 1.29% and 7.06%, respectively, and in comparison to the value obtained from experimentation, the GGA-PBE method is the most consistent with the experimental value[10], which shows that this method is the most consistent. At the same time, we found that LDA is the only method that calculates the value less than the experimental value, and overestimating the energy will result in the calculated value less than the experimental value, therefore, LDA has been abandoned in this work after testing, so GGA-PBE will be used next in this work for calculation.

3.2. Elastic properties

In the next section, we will use the well-established unit cell structure model of Cu_2ZnSnS_4 to explore the elastic properties of Cu_2ZnSnS_4 under different pressures, such as 0GPa, 5GPa, 10GPa, 15 GPa, 20 GPa, the stability condition of Born must be satisfied [11]. The mechanical stability conditions are met by the elastic constants, indicating that the Cu_2ZnSnS_4 structure exhibits mechanical stability. The obtained elastic constants are consistent with previously reported theoretical values [6, 12], confirming the accuracy of our calculation. Fig. 2 shows that the elastic properties of Cu_2ZnSnS_4 are primarily categorized into three distinct groups: the first group is C_{11} and C_{33}, the second group is C_{12} and C_{13}, and the third group is C_{44} and C_{66}. First, we look at the first group, C_{11} and C_{33} are increasing with increasing pressure, but the speed is slightly different, at 0-5 GPa, C_{11} is increasing faster than C_{33}, at 5-15 GPa, C_{11} rises at about the same rate as C_{33}, and at 15-20 GPa, C_{11} rises faster than C_{33}. Then we looked at the second group, where C_{12} and C_{13} rose at almost the same rate over the entire range of 0-20 GPa, but C_{13} was still slightly larger than C_{12} over the range of 0-5 GPa, and the rise rate of C_{12} and C_{13} was slightly larger over the range of 5-10 GPa, at 10-15 GPa, however, the rise of C_{12} and C_{13} was slightly smaller, and at 15-20 GPa, the rise of C_{12} and C_{13} was much larger. Finally, let's look at the third group, which has a much smaller change compared with the first and second groups, indicating that stress does not have a significant effect on these two data, with a slight increase in C_{44} and C_{66} at 0-5 GPa and a slight increase at 5-15 GPa, the rate of decline of C_{44} was slightly higher than that of C_{66}, and the rate of decline of C_{44} was slightly lower than that of C_{66} at 15-20 GPa.

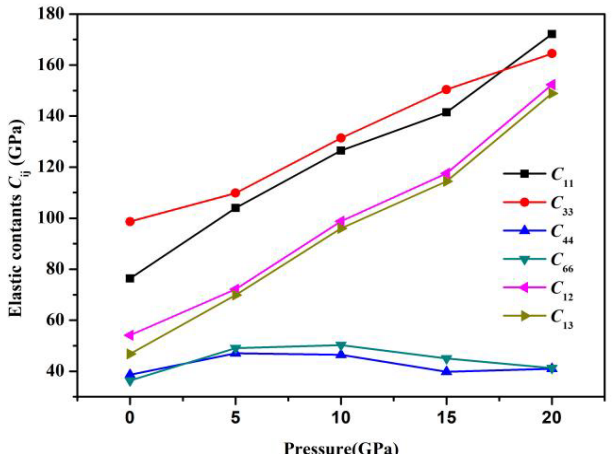

Fig. 2. The impact of pressure on Cu_2ZnSnS_4's C_{ij} under varying pressure conditions.

Table 2. Calculated elastic constants C_{ij} (GPa), B (GPa), G (GPa), E(GPa), Poisson ratio υ, B/G of Cu_2ZnSnS_4 at different pressures.

Pressure(GPa)	C_{11}	C_{33}	C_{44}	C_{66}	C_{12}	C_{13}	B	G	E	B/G	υ
0	76.41	98.69	38.64	36.30	54.12	46.78	60.59	26.62	69.65	2.28	0.31
0 [6]	102.39	127.09	24.19	29.70	46.50	35.26	62.60	29.87	77.31		0.294
0 [12]	121.03	113.36	28.40	27.40	52.51	64.07	76.61	30.79			
5	103.99	109.81	47.03	49.03	72.13	69.90	82.39	31.93	84.84	2.58	0.33
10	126.47	131.38	46.43	50.21	98.80	96.01	107.33	30.38	83.28	3.52	0.37
15	141.43	150.37	39.80	45.00	117.54	114.45	125.09	26.977	75.50	4.64	0.40
20	172.11	164.48	40.97	41.24	152.35	148.85	156.29	23.265	66.50	6.72	0.43

In Fig.3, the graphical representation illustrates the variations in *B*, *G*, and *E*. The initial parameter to consider is the *B*, which exhibits a significant increase in value as pressure rises within the range of 0 to 20 GPa. This increase surpasses that observed for both *G* and *E*. The trend of *G* was similar to *E*, which increased slightly at 0-5 GPa and decreased slightly at 5-20 GPa. Compared with the *B*, the change of *G* and *E* is very small.

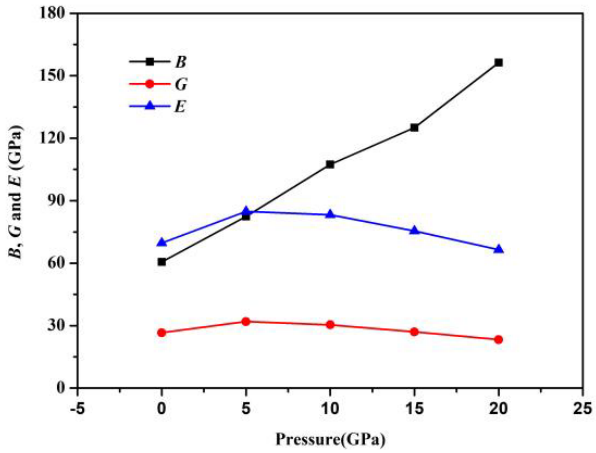

Fig. 3. The impact of pressure on the B, G, and E of Cu_2ZnSnS_4 with respect to varying pressure conditions.

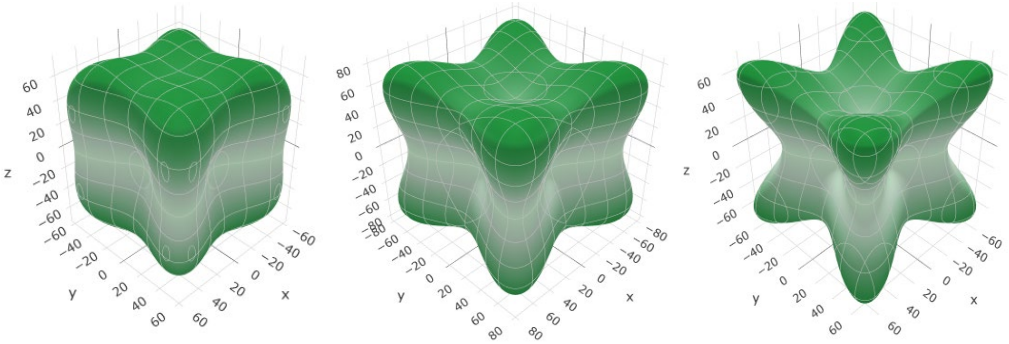

(0GPa) *(10GPa)* *(20GPa)*

Fig. 4. The representation of E(GPa) in three-dimensional space of Cu_2ZnSnS_4.

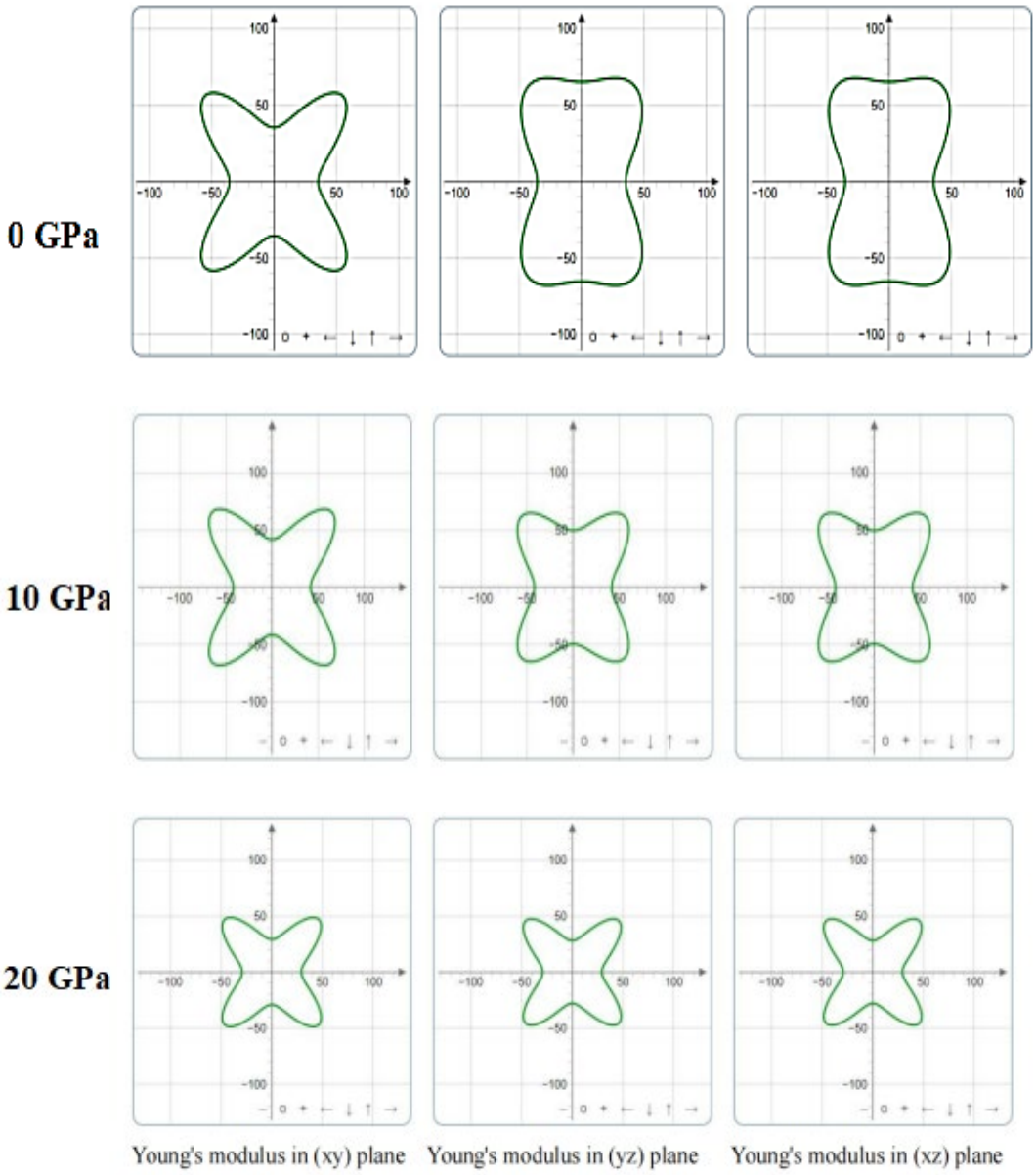

Fig. 5. The representation of E (GPa) in the different planes of Cu_2ZnSnS_4.

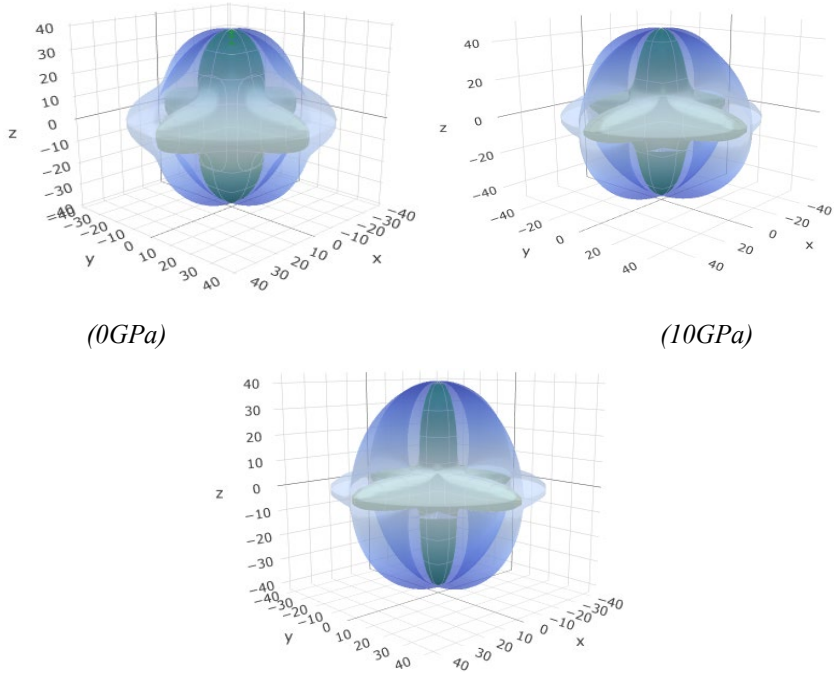

(0GPa) *(10GPa)*

(20GPa)

Fig. 6. The representation of G (GPa) in three-dimensional space of Cu_2ZnSnS_4.

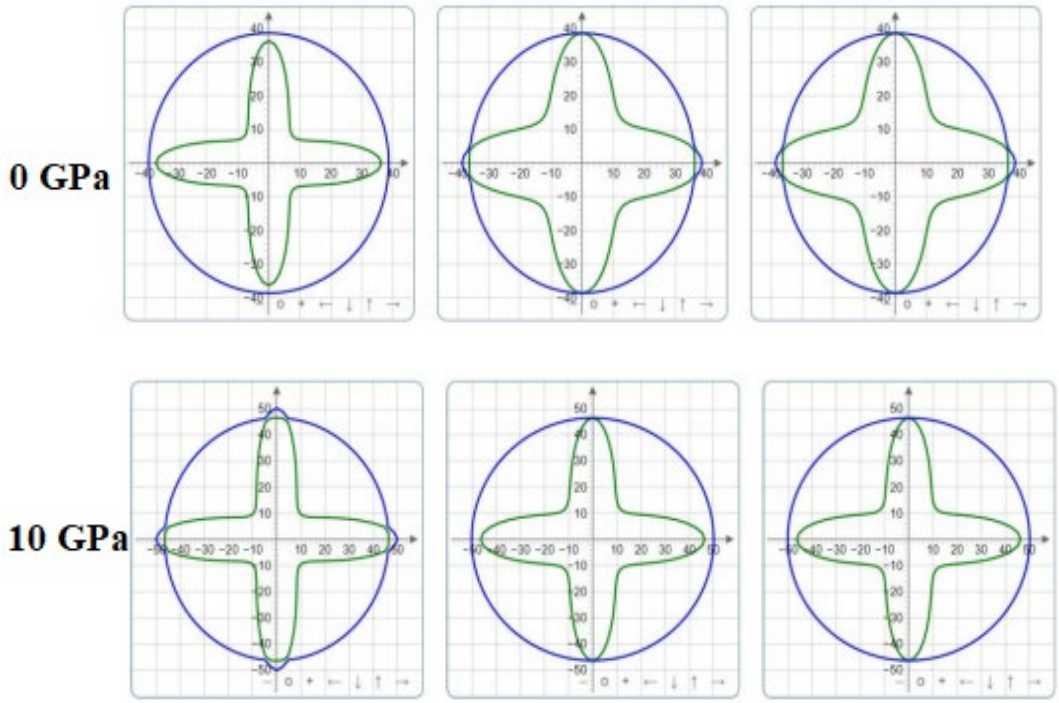

Fig. 7.1 The representation of G(GPa) in the different planes of Cu_2ZnSnS_4.

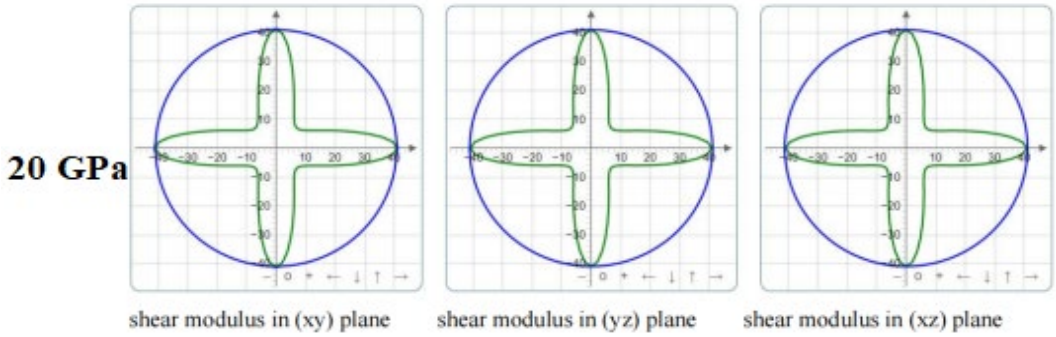

Fig. 72. The representation of G(GPa) in the different planes of Cu_2ZnSnS_4.

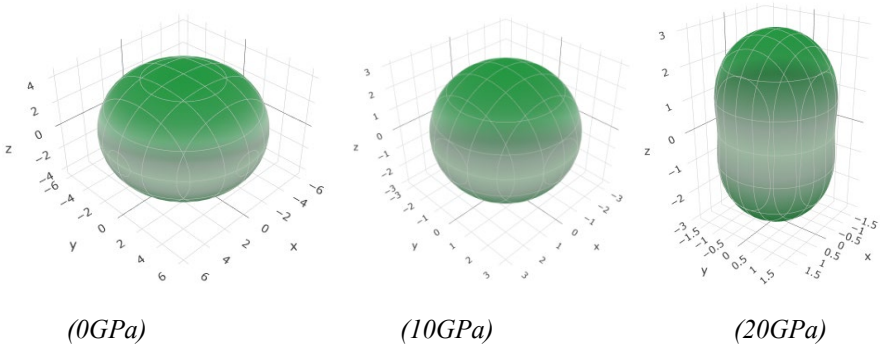

Fig. 8. The representation of β(TPa^{-1}) in three-dimensional space of Cu_2ZnSnS_4.

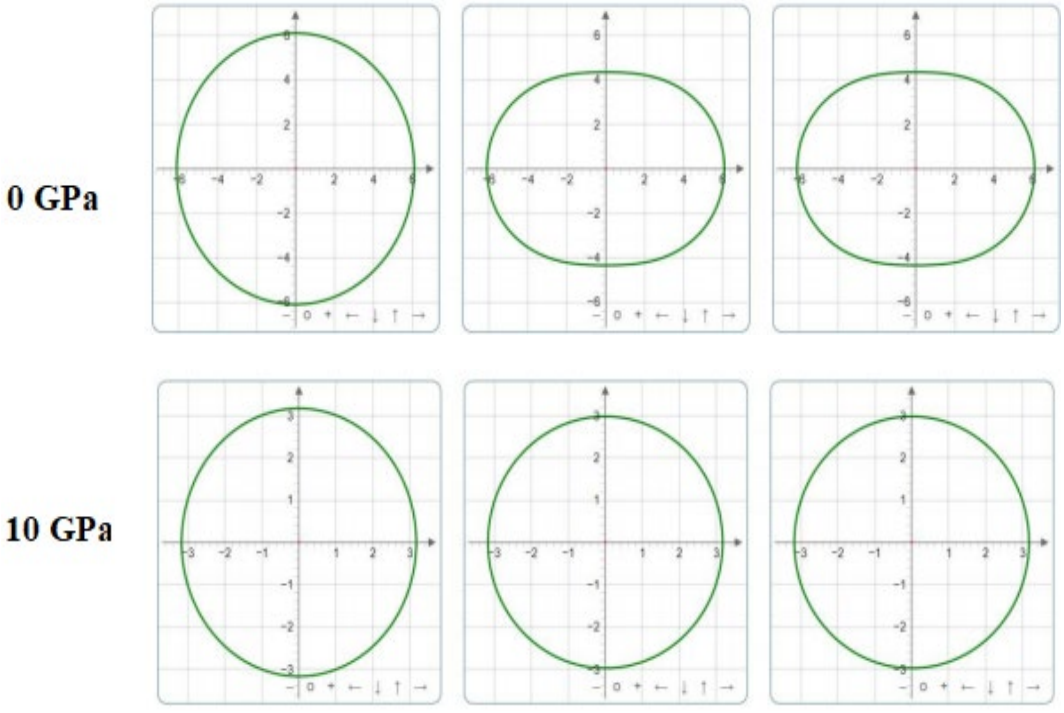

Fig. 9.1 The representation of β (TPa^{-1}) in the different planes of Cu_2ZnSnS_4.

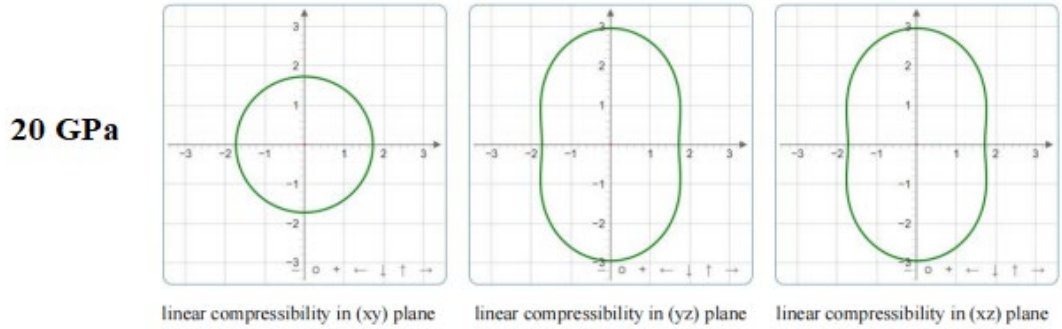

Fig. 9.2 The representation of β (TPa^{-1}) in the different planes of Cu_2ZnSnS_4.

According to the Pugh criterion, the ductility or brittleness of a solid material is determined by the ratio of *B*/*G*. If *B*/*G* is less than 1.75, the solid exhibits brittleness. Conversely, when the ratio exceeds 1.75[13], it indicates a ductile nature of the material. According to the information in Table 2, it can be deduced that Cu_2ZnSnS_4 exhibits ductility. In order to fully understand the anisotropy of Cu_2ZnSnS_4, we try to determine the three-dimensional (3D) surface structure of Cu_2ZnSnS_4 based on its linear compressibility *β*, *G*, *E* [14]. Figs. 4-9 show the in 3D space and representation in different planes of elastic modulus (*β*, *G*, *E*) at specific pressure, it is obvious that the difference between the spherical shape and the 3D image is very large except for *β* of elasticity, which indicates that the 3D image has remarkable anisotropy. The *β* of elasticity is different from that of sphere at 0 GPa and 20 GPa, except that it approaches sphere at 10 GPa. The estimations of *E*, *G*, and *β* in the xy, xz, and yz planes. The anisotropy increases as the deviation from the circle becomes greater. The crystal planes of Cu_2ZnSnS_4 exhibit significant deviations from circular shapes, providing further evidence for the pronounced anisotropy of this material. The *β* is nearly circular in all three planes except for 20 GPa, and elliptic in yz plane and xz plane at 20 GPa.

3.3. Thermal properties

First, the total energy *E* of Cu_2ZnSnS_4 with its corresponding volume *V* through MS-related data and Birch-Murnaghan equation of state [15], and made *E*-*V* based on relevant data, as shown in Fig. 10. From the graph, it is evident that at a volume of 2168.21 $Bohr^3$, the energy reaches its minimum value of -309.53537 Hartree.

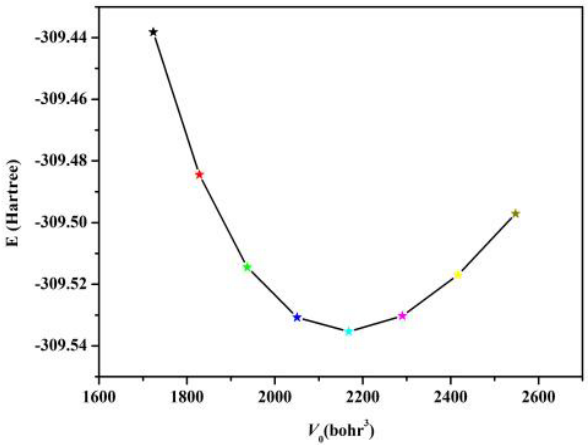

Fig. 10. Calculated total energy E and volume V of Cu_2ZnSnS_4.

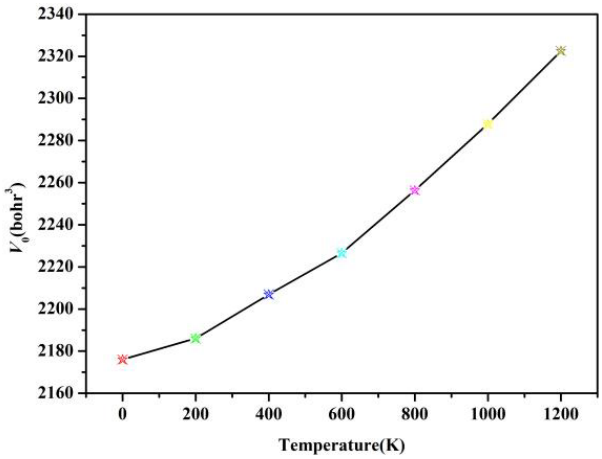

Fig. 11. The volume V changes with temperature at zero pressure.

Fig. 11 shows the temperature *T* and its corresponding volume *V* at zero pressure. From the graph, we can see that with the increasing of temperature *T*, the volume *V* increases gradually, the overall trend of increase does not change much, but the overall trend is accelerating. At 0-200K, the rate of rise was the slowest, at 200-400K, it began to accelerate, and at 600-1200K, it accelerated, but the range was not as large as 200-400K.

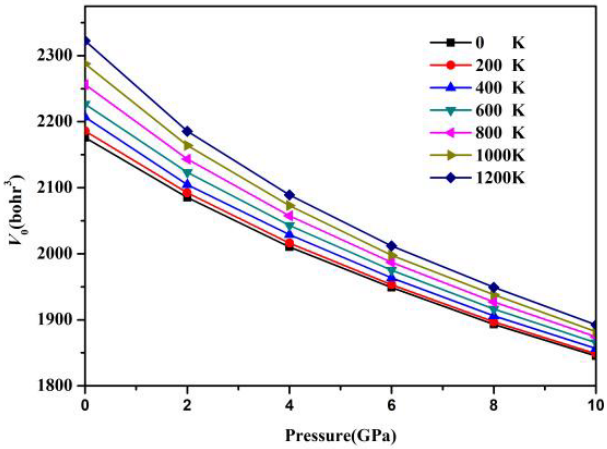

Fig. 12. The volume changes with pressure at (0, 200, 400, 600, 800, 1000, 1200K), respectively.

Fig.12 shows the volume V changes with pressure at (0, 200, 400, 600, 800, 1000, 1200K), respectively. The volume V of Cu_2ZnSnS_4 at various temperatures decreases with increasing pressure P. As a whole, the lower the temperature, the faster the volume decline. At 0-2 GPa, their values are quite different of each temperature, but with the increasing pressure, the falling velocity tends to be the same gradually, at 6 GPa-10 GPa, the falling curve is almost parallel.

Fig. 13 shows the C_V changes with temperature at (0, 2, 4, 6, 8, 10 GPa), respectively. There is a positive correlation between temperature T and the C_V. There is little variation in the increasing trend between different curves, but there are subtle differences. At 0-200 K, the increase of C_V is much larger than that at 200-1200 K, and it decreases with the increase of pressure, the growth rate of C_V is obviously decreased, and 0 GPa is the slowest at this time. With the increase of pressure, the growth rate of C_V increases continuously. Therefore, all the curves coincide gradually, and finally converge to the same value, this value is the Dulong-Petit limit.

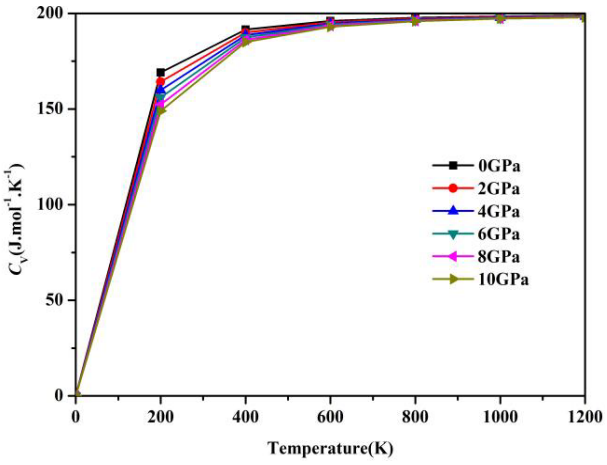

Fig. 13. The C_V changes with *temperature at (0, 2, 4, 6, 8, 10 GPa), respectively.*

The C_P changes with temperature at (0, 2, 4, 6, 8, 10 GPa) is illustrated in Fig.14. As the temperature T rises, there is a noticeable increase in the heat capacity C_P. The overall trend remains relatively consistent across different curves, although subtle distinctions can be observed. At 0-200 K, the growth rate of heat capacity C_P is much larger than that at 200-1200 K, at which time the growth rate of 0GPa is the fastest, the growth rate of heat capacity C_P is obviously decreased, and 0 GPa is the slowest at this time. With the increase of pressure, its growth rate increases continuously, and at 400-1200K, the growth rate of 0 GPa is the fastest.

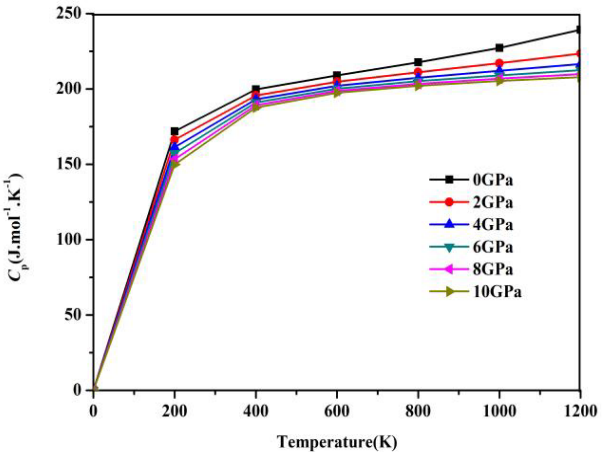

Fig. 14. The C_P changes with *temperature at (0, 2, 4, 6, 8, 10 GPa), respectively.*

Fig. 15 plots the α changes with temperature at (0, 2, 4, 6, 8, 10 GPa), respectively. As depicted in the graph, there is a noticeable correlation between temperature T and α, with an observed increase as temperature rises. Moreover, it is worth noting that the curves exhibit a strikingly similar trend. At 0-200K, the growth rate of α is much larger than that at 200-1200 K. At this time, the growth rate of 0 GPa is the fastest, at 200-400K, the α increases at 10 GPa, but at 400-600 K, it increases the most as the pressure decreases, the growth rate of α decreased from 600 to 1200 K, and the growth rate of the volume fraction was the fastest at 0 GPa. Fig. 16 shows the α changes with pressure at (0, 200, 400, 600, 800, 1000, 1200 K), respectively. The α of Cu_2ZnSnS_4 at each temperature decreases as the pressure P increases (except for 0 K, where the α is always 0). In general, as the temperature increases, there is a corresponding decrease in the α. The rate of decrease in the α is highest at 2 GPa and diminishes as the temperature increases.

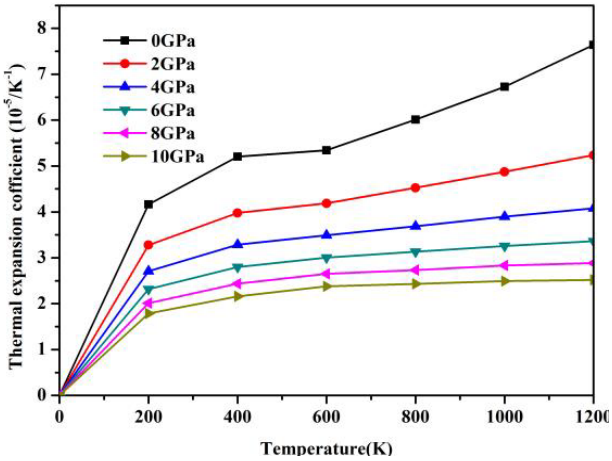

Fig. 15. The α changes with temperature at (0, 2, 4, 6, 8, 10 GPa), respectively.

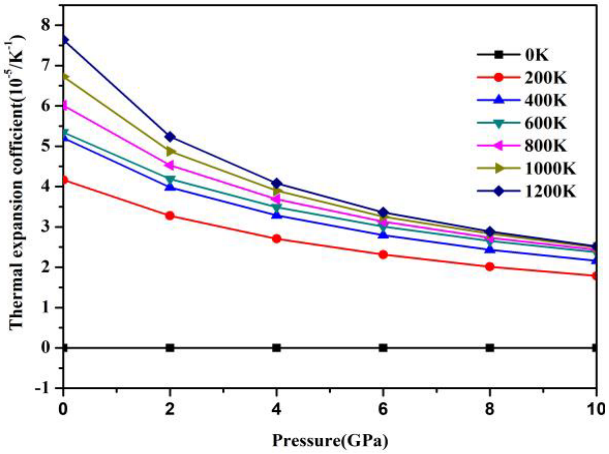

Fig. 16. The α changes with pressure at (0, 200, 400, 600, 800, 1000, 1200 K), respectively.

Table 3. The calculated S, θ, and γ of Cu_2ZnSnS_4 under varying pressures (0, 2, 4 , 6, 8, 10 GPa) and temperatures (0, 200, 400, 600, 800, 1000, 1200K).

T/K	*P*/GPa	0	2	4	6	8	10
0	*S*	0	0	0	0	0	0
	θ	373.99	405.79	433.56	457.57	480.37	500.59
	γ	1.98	1.857	1.768	1.7	1.643	1.597
200	*S*	159.14	145.06	134.12	125.42	117.85	111.55
	θ	370.59	403.23	431.38	455.81	478.76	499.22
	γ	1.995	1.866	1.774	1.705	1.647	1.6
400	*S*	289.18	271.48	258.80	248.01	238.66	230.67
	θ	363.57	398.91	426.56	451.74	474.93	495.84
	γ	2.026	1.882	1.789	1.716	1.656	1.608
600	*S*	371.40	353.01	339.06	327.45	317.53	308.95
	θ	357.04	392.22	421.31	447.22	470.7	492.06
	γ	2.056	1.907	1.805	1.728	1.667	1.616
800	*S*	433.49	413.02	397.95	385.75	375.44	366.49
	θ	347.33	385.28	415.88	442.5	466.36	488.14
	γ	2.104	1.934	1.823	1.741	1.677	1.625
1000	*S*	483.54	460.83	444.71	431.58	421.24	411.67
	θ	337.23	378.15	410.23	438.38	461.95	484.9
	γ	2.158	1.962	1.842	1.753	1.689	1.633
1200	*S*	526.30	500.91	483.70	470.12	459.23	449.48
	θ	326.29	370.76	404.34	433	457.46	480.54
	γ	2.22	1.994	1.862	1.769	1.7	1.643

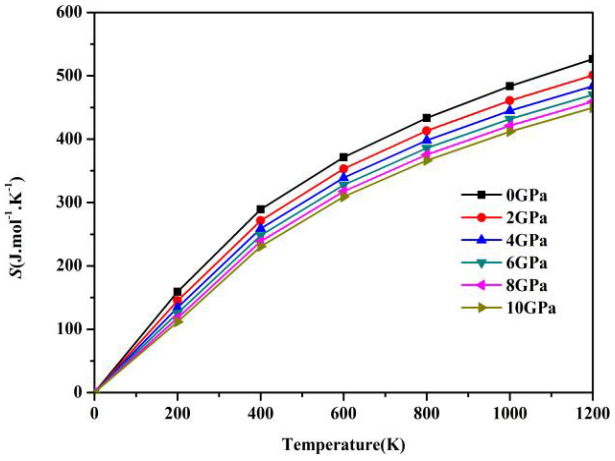

Fig. 17. The pressure dependence of entropy at (0, 2, 4 , 6, 8, 10 GPa), respectively.

The pressure dependence of *S* at (0, 2, 4 , 6, 8, 10 GPa) is illustrated in Fig.17. As you can see from the graph, the *S* increases with increasing temperature *T*, and the trend is very similar between the curves. As a whole, *S* increases fastest at 0 GPa, and decreases with increasing pressure, and increases with increasing temperature. Fig. 18 depicts the correlation between *P* and *θ* under different temperature conditions. As depicted in the graph, there is a positive correlation between pressure *P* and the *θ*, indicating an increase in the latter with an increase in the former. On the whole, *θ* at 1200 K increased the fastest, and as the temperature decreased, its growth rate decreased, and as the pressure increased, its growth rate gradually decreased.

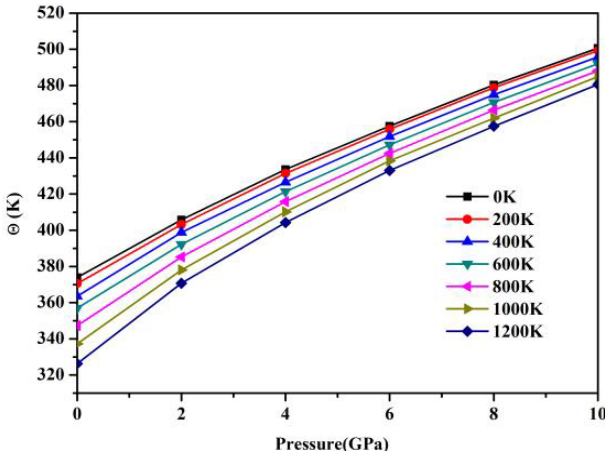

Fig. 18. The θ changes with pressure at (0, 200, 400, 600, 800, 1000, 1200 K) , respectively.

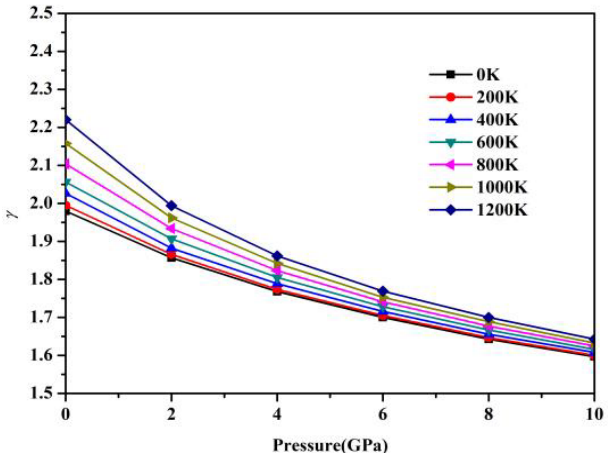

Fig. 19. The γ changes with pressure at (0, 200, 400, 600, 800, 1000, 1200 K) , respectively.

Fig.19 plots the γ changes with pressure at (0, 200, 400, 600, 800, 1000, 1200 K), respectively. The γ decreases with increasing pressure P, and the increasing trend is very similar between different curves. Overall, θ dropped fastest at 1200K, decreasing as the temperature dropped and decreasing as the pressure increased. Furthermore, the S, θ, and γ of Cu_2ZnSnS_4 under varying temperatures and pressures are presented in Table 3. The anticipated outcomes will offer valuable insights for exploring novel functional materials and their potential applications.

4. Conclusions

Utilizing DFT, we have developed and fine-tuned a structural representation of Cu_2ZnSnS_4, commonly known as chalcopyrite, to investigate its thermodynamic and elastic characteristics. The calculations were performed to study the B, G, E, and υ. The strong elastic anisotropy of Cu_2ZnSnS_4 is evident from the analysis of β, G, E three-dimensional surface structures, and

representation in the different planes. The temperature and pressure-dependent properties of Cu_2ZnSnS_4, including the θ, C_V and C_P, α, γ, and S were determined through calculations.

References

[1] C.Wadia, A. P. Alivisatos, D. M. Kammen, Environ. Sci. Technol., 2009, 43: 2072; https://doi.org/10.1021/es8019534

[2] K. Kaur, N. Kumar, M. Kumar, J. Mater. Chem. A 5 (2017)3069; https://doi.org/10.1039/C6TA10543B

[3] S. N. Park, S. J. Sung, K. J. Yang, J. K. Kang, D. H. Kim, J. Nanosci Nanotechno. 10 (15) (2016) 10490; https://doi.org/10.1166/jnn.2016.13182

[4] A. Walsh, S. Chen, S. H. Wei, Adv. Energy Mater., 2012, 2: 400; https://doi.org/10.1002/aenm.201100630

[5] A. P. Chowdhury, B. H. Shambharkar, Appl. Water Sci. 26(2018) 076201; https://doi.org/10.1007/s13201-018-0853-0

[6] Y.F. Zhao, D.C. Li, Z.M. Liu, J. Alloy. Compd. 696 (2017) 86; https://doi.org/10.1016/j.jallcom.2016.11.091

[7] S. J. Clark, M. D. Segall, C. J. Pickard, Z. Kristallogr 220(2005) 567; https://doi.org/10.1524/zkri.220.5.567.65075

[8] J.P. Perdew, K. Burke, M. Ernzerhof, Phys. Rev. Lett.77(1996)3865; https://doi.org/10.1103/PhysRevLett.77.3865

[9] D. Vanderbilt, Phys. Rev. B 41(1990)7892; https://doi.org/10.1103/PhysRevB.41.7892

[10] X.Y. Shi, F.Q. Huang, M.L. Liu, L.D. Chen, Appl. Phys. Lett. 94 (2009) 122103; https://doi.org/10.1063/1.3103604

[11] M. Born, K. Huang, Dynamical Theory of Crystal Lattices (Oxford: Clarendon) 1954.

[12] T. Gürel, C. Sevik, T. Cagin, Phys. Rev. B 84 (2011) 205201; https://doi.org/10.1103/PhysRevB.84.205201

[13] S. F. Pugh, Philos. Mag. 45, 823 (1954); https://doi.org/10.1080/14786440808520496

[14] R. Gaillac, P. Pullumbi, F.-X. Coudert, J. Phys. Condens. Matter 28, 275201(2016); https://doi.org/10.1088/0953-8984/28/27/275201

[15] M. A. Blanco, A. Martín Pendás, E. Francisco, J. M. Recio, R.Franco, J. Mol. Struc-Theochem. 368, 245(1996); https://doi.org/10.1016/S0166-1280(96)90571-0